Corrosion inhibition of mild steel by triazole and thiadiazole derivatives in 5 M hydrochloric acid medium

M.D. Plotnikova,* A.D. Solovyev, A.B. Shein, A.N. Vasyanin and A.S. Sofronov

Perm State National Research University, st. Bukireva 15, 614068 Perm, Russian Federation
**E-mail: plotnikova-md@mail.ru*

Abstract

The article presents the results of studies on triazole and thiadiazole derivatives as corrosion inhibitors for mild steel in 5 M hydrochloric acid solution. 2-Amino-1,3,4-thiadiazole with tall oil fragments, namely, 3,4-diphenyl-5-(prop-2-yn-1-ylthio)-4*H*-1,2,4-triazole, and 2-(3,5-diphenyl-4,5-dihydro-1*H*-pyrazole-1-yl)-5-phenyl-1,3,4-thiadiazole, were studied. The protonation of the studied molecules in hydrochloric acid medium was calculated using semi-empirical GFN2-xTB Grimme's method. Weight loss measurements were carried out on C1018 steel at a temperature of 293 K and 24 h exposure time. Polarization curves were recorded in the temperature range of 293–353 K in potentiodynamic mode in a three-electrode cell from cathodic to anodic potentials at a potential sweep rate of 0.5 mV/s using a SOLARTRON 1280 C electrochemical measuring complex. It was found that 2-(3,5-diphenyl-4,5-dihydro-1*H*-pyrazole-1-yl)-5-phenyl-1,3,4-thiadiazole had the maximal inhibition effect in 5 M HCl solution (~97% at concentrations >50 mg/L). 3,4-Diphenyl-5-(prop-2-yn-1-ylthio)-4*H*-1,2,4-triazole had the minimum protective properties among the compounds studied, as its inhibition effect reached 80–90% in the concentration range studied. The compounds studied are mixed-type (2-amino-1,3,4-thiadiazole with a tall oil fragment and 2-(3,5-diphenyl-4,5-dihydro-1*H*-pyrazole-1-yl)-5-phenyl-1,3,4-thiadiazole) or cathodic-type inhibitors (3,4-diphenyl-5-(prop-2-yn-1-ylthio)-4*H*-1,2,4-triazole). The results of weight loss and electrochemical measurements agree both qualitatively and quantitatively. 2-(3,5-Diphenyl-4,5-dihydro-1*H*-pyrazole-1-yl)-5-phenyl-1,3,4-thiadiazole retains its high protective effect at elevated temperatures because its molecule has significantly more conjugated electron clouds. Addition of the inhibitors to a corrosive medium increases the effective activation energy of the corrosion process. This fact indicates physical adsorption of the inhibitor molecules on the electrode surface. The degrees of surface coverage of steel with triazole molecules were estimated from the results of electrochemical impedance spectroscopy at the corrosion potential. The adsorption process was found to obey the Langmuir equation. The results show that it is promising to search for potential acid corrosion inhibitors among a number of triazole and thiadiazole derivatives.

Received: September 15, 2021 Published: September 21, 2021 doi: 10.17675/2305-6894-2021-10-3-29

Keywords: *mild steel, acid corrosion, thiadiazole, triazole, inhibitor, potentiodynamic polarization, activation energy, electrochemical impedance spectroscopy, adsorption.*

1. Introduction

Iron and its alloys are widely used in many areas of industry. It contacts various corrosive media and it is essential to study its corrosion resistance [1]. Among the various available methods of corrosion damage control, inhibitors provide the most accessible option [2–4]. This method is based on isolating a metal surface from the corrosive agents. Inhibition occurs due to the adsorption of organic molecules on the metal surface [5]. The adsorption film of inhibitors acts as a barrier protecting the metal from the corrosive environment, and the inhibition efficiency depends on the structural and chemical characteristics of the adsorption layers [6, 7].

The most effective organic inhibitors comprise heteroatoms with high electron density (P, S, N and O) or aromatic rings and conjugated systems as adsorption centers [8–10]. Indeed, some N-heterocyclic compounds, such as thiadiazoles, triazoles, oxadiazoles, benzimidazoles, etc. are well known as effective corrosion inhibitors of mild steels in a number of corrosive environments [11–14]. High protective properties are usually provided by chelate complexes formed with the metal.

Currently, 1,3,4-thiadiazole derivatives are being studied as corrosion inhibitors of mild steel. The aim of this article is to study 1,3,4-thiadiazoles containing a tall oil fragment, namely, 3,4-diphenyl-5-(prop-2-yn-1-ylthio)-4*H*-1,2,4-triazole, and 2-(3,5-diphenyl-4,5-dihydro-1*H*-pyrazole-1-yl)-5-phenyl-1,3,4-thiadiazole, as new corrosion inhibitors of C1018 steel in 5 M HCl solution. They were chosen as potential inhibitors for a number of reasons. First, it is the environmental friendliness and cheapness of their synthesis. Second, they comprise heteroatoms, such as N and S, and a phenyl ring with conjugated π-electrons. These structural features favor the adsorption of the inhibitors on the metal surface, thus contributing to effective protection.

2. Experimental

2.1. Synthesis of inhibitors

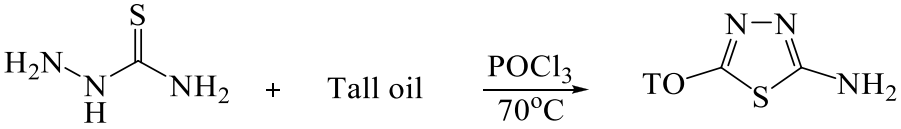

Figure 1. Synthesis scheme of 1,3,4-thiadiazole containing a tall oil fragment (CP-16).

Tall oil was subjected to $POCl_3$-mediated cyclization with thiosemicarbazide to give 5-substituted 2-amino-1,3,4-thiadiazole.

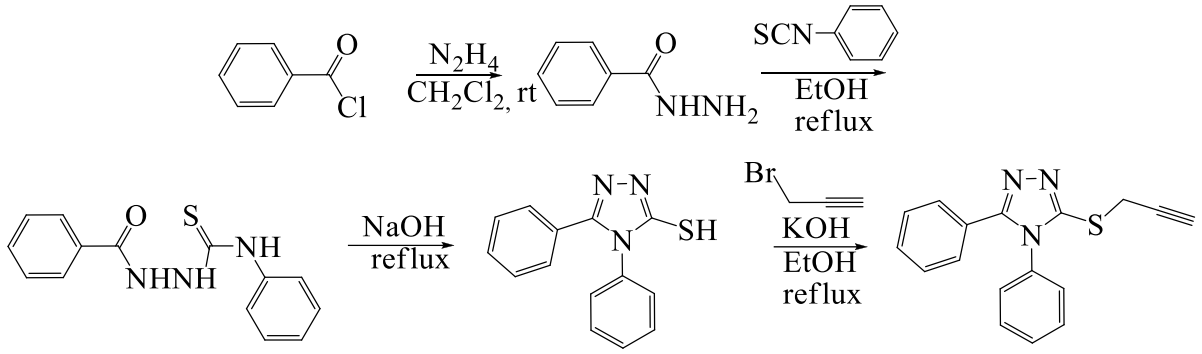

Figure 2. Synthesis scheme of 4-diphenyl-5-(prop-2-yn-1-ylthio)-4*H*-1,2,4-triazole (CP-41).

Compound CP-41 was prepared by the methods shown in the scheme. Benzoyl hydrazide was synthesized by the reaction of benzoyl chloride with hydrazine hydrate. The reaction of benzoyl hydrazide with phenyl isothiocyanate gave the corresponding 1-benzoyl-4-phenyl-3-thiosemicarbazide. The corresponding thiosemicarbazide was cyclized to 4,5-disubstituted-4*H*-1,2,4-triazole-3-yl-thiol in the presence of 10% aqueous sodium hydroxide. Further, we prepared the propargyl derivatives of 3-mercapto-1,2,4-triazole synthesized by alkylation of triazoles with propargyl bromide under basic conditions.

^{1}H NMR (400 MHz, DMSO d_6) δ 7.27–7.28 (m, 3H, Ph), 7.13–7.15 (d, *J*=7.9 Hz, 2H, Ph), 7.03–7.05 (m, 2H, Ph), 6.96–6.93 (t, *J*=7.2 Hz, 2H, Ph), 6.31–6.66 (t, *J*=7.4 Hz, 1H, Ph), 3.53 (s, 1H, CH_2), 1.90 (s, 1H, ≡CH). ^{13}C NMR (400 MHz, DMSO d_6) δ 151.82, 144.97, 139.21, 131.79, 130.60, 130.52, 129.12, 127.57, 122.15, 117.38, 78.43, 72.43, 21.55.

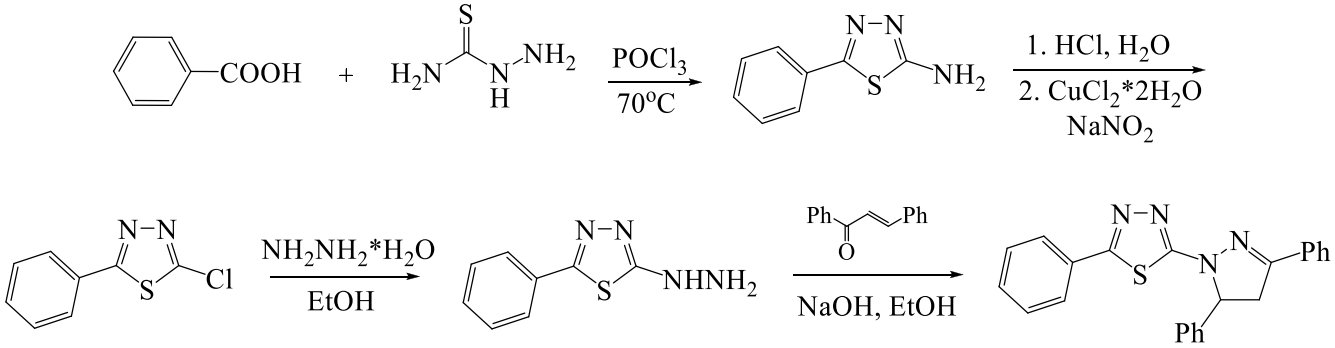

Figure 3. Synthesis scheme of 2-(3,5-diphenyl-4,5-dihydro-1*H*-pyrazole-1-yl)-5-phenyl-1,3,4-thiadiazole (CP-44).

2-Amino-5-phenyl-1,3,4-thiadiazole was obtained by direct cyclization of a carboxylic acid and thiosemicarbazide. The amino-heterocyclic derivative was converted into the corresponding chlorides by the diazotization and Sandmeyer reaction with $CuCl_2$ generated *in situ*. Then, 1,3,4-thiadiazolyl chloride was subjected to an aromatic nucleophilic substitution reaction with excess hydrazine hydrate in ethanol to give the corresponding heteroarylhydrazine in a good yield. Further, a pyrazoline compound containing 5-phenyl-1,3,4-thiadiazole groups at position 1 was synthesized by cyclization of chalcone and 5-phenyl-2-hydrazinyl-1,3,4-thiadiazole.

^{1}H NMR (400 MHz, DMSO d_6) δ 3.23–3.29 (dd, 1H, *J*=17.6, 6.2 Hz, pyrazoline), 3.81–3.88 (dd, 1H, *J*=17.6, 11.9Hz, pyrazoline), 5.63–5.68 (dd,1H, *J*=11.9, 6.12 Hz, pyrazoline), 7.13–7.16 (m, 2H, Ph), 7.20–7.23 (t, 2H, *J*=7.4, Ph), 7.27–2.28 (m, 4H, Ph), 7.31–7.32 (m, 3H, Ph), 7.63–7.65 (dd, 2H, *J*=6.6, 2.9 Hz, Ph), 7.69–7.71 (dd, 2H, *J*=7.3, 2 Hz, Ph). ^{13}C NMR (400 MHz, DMSO d_6) δ 43.71, 64.22, 126.08, 126.27, 126.63, 127.77, 128.49, 128.59, 128.66, 129.63, 130.01, 130.63, 140.23, 153.53, 159.55, 165.40.

2.2. Quantum chemical calculations

The presence of nitrogen atoms in the molecules of CP-16, CP-41 and CP-44 inhibitors gives them basic properties in aqueous solutions. A semi-empirical calculation was performed using the GFN2-xTB Grimme method [15, 16] to determine the protonation sequence of individual atoms taking implicit solvation in an aqueous medium into account.

2.3. Weight loss measurements

Samples of mild steel C1018 with the composition, wt.%: Fe–98.27; C–0.20; Mn–0.50; Si–0.30; P–0.04; S–0.04; Cr–0.15; Ni–0.30; Cu–0.20, were used in the study. The experiments were carried out in 5 M HCl solutions prepared from distilled water and 37% HCl. Organic synthesis products – triazole and thiadiazole derivatives – were used as the corrosion inhibitors (Table 1).

A microscopic examination of the mild steel surface was carried out after the weight loss tests using an Olympus optical microscope.

Table 1. Nitrogen-containing heterocycles studied in this work as corrosion inhibitors.

Code	Formula	Name according to nomenclature
CP-16	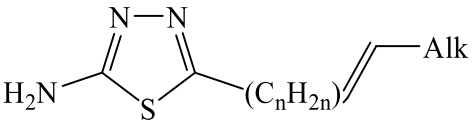	2-amino-1,3,4-thiadiazole containing a tall oil fragment
CP-41	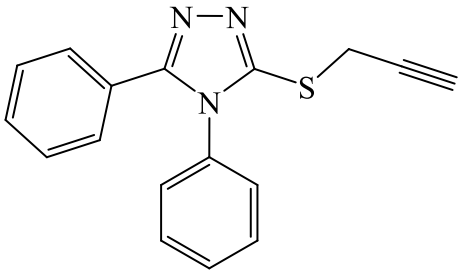	3,4-diphenyl-5-(prop-2-yn-1-ylthio)-4*H*-1,2,4-triazole
CP-44	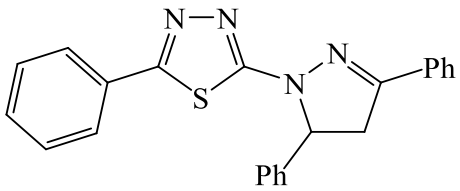	2-(3,5-diphenyl-4,5-dihydro-1*H*-pyrazole-1-yl)-5-phenyl-1,3,4-thiadiazole

The main parameters of C-steel corrosion were estimated by generally accepted methods [17]. Weight loss tests were carried out using rectangular plates made of C1018 steel with dimensions of 25×20×2 mm. The working surface area was 1180 mm^2.

The corrosion rates (K and Π), degree of inhibition (γ) and degree of protection (Z_{wl}) were calculated using the equations:

$$K = \frac{m_0 - m}{S \cdot \tau}$$

$$\Pi = \frac{K}{\rho} \cdot 8.67$$

$$\gamma = \frac{K_0}{K}$$

$$Z_{wl} = \frac{K_0 - K}{K_0} \cdot 100\%$$

where m_0 is the mass of the initial sample, g; m is the mass of the sample after corrosion testing and removal of corrosion products, g; S is the surface area of the sample, m^2; τ is the immersion time, h; K_0 and K are the corrosion rates of steel, respectively, in the pure solution and with addition of an inhibitor, in g/(m^2 h).

2.3. Electrochemical measurements

A Solartron 1280C measuring complex (Great Britain) consisting of an impedance analyzer SI 1255 and a potentiostat SI 1287 and a three-electrode cell with separate cathode and anode spaces were used for electrochemical studies.

The polarization curves were recorded by the potentiodynamic technique from the cathodic to the anodic region at a scanning rate of 0.5 mV/s. All the potentials are presented *versus* the silver chloride electrode.

Polarization measurements were carried out in the temperature range from 293 to 353 K. The cell was connected with a LOIP LT 100 thermostat with external circulation to maintain the required temperature.

Before each electrochemical experiment, the electrode surface was cleaned with sand paper and then degreased with acetone.

The method of polarization curves allows one to calculate the corrosion rate (i_{corr}) in current density units, the corrosion potential (E_{corr}), and to determine the type of the inhibitor, *i.e.* which of the partial electrode reactions (hydrogen evolution or metal ionization) is mainly hindered by the inhibitor. This method also allows one to determine the Tafel sections of the polarization curves and calculate the degree of protection from electrochemical data [18]:

$$Z_{el} = \frac{i_0 - i_{inh}}{i_0} \cdot 100\%$$

where i_0 and i_{inh} are the current densities of steel corrosion, respectively, in the pure solution and with addition of an inhibitor, in A/m^2.

Based on the electrochemical results, the activation energy of the corrosion process was calculated. The calculations were performed by the temperature-kinetic method. The effect of temperature on the current density in cases of concentration polarization or delayed discharge stage is described by an equation similar to the Arrhenius equation [19]:

$$\ln i = -\frac{E_{ef}}{RT}$$

where i is the corrosion current density, A/m^2; E_{ef} is the effective activation energy of the corrosion process, J/mol; T is the temperature, K.

A straight line in the $\lg(i) = f(1/T)$ coordinates allows E_{ef}/R to be calculated as the slope.

The surface coverage (θ) of the C1018 electrode by a corrosion inhibitor was determined from the equation:

$$\theta = \frac{C_0 - C}{C_0 - C_1}$$

where C_0, C and C_1 are, respectively, the capacitance of the double electric layer in the pure acid solution, in the solution with a given concentration of the inhibitors, and in the solution with $\theta = 1$. The value of C_1 was determined by extrapolating the curve in the coordinates $C = f\left(\frac{1}{C_{inh}}\right)$ to $\left(\frac{1}{inh}\right) = 0$, where C_{inh} is the inhibitor concentration in the solution, mg/L.

All the data presented in this work was obtained by averaging the results of three parallel measurements. MS Excel software was used to calculate the average results and standard deviations of direct and indirect measurements.

3. Results and Discussion

The nitrogen atoms in the CP-16, CP-41 and CP-44 inhibitor molecules have basic properties in aqueous solutions according to quantum chemical calculations. A semi-empirical calculation was performed using Grimme's GFN2-xTB method to determine the protonation sequence of individual atoms, taking into account implicit solvation in an aqueous medium.

The tall oil fragment in the molecule is replaced by the C_{10} alkyl radical. Protonation of CP-16 occurs at the first and second stages at the nitrogen atoms of the heterocycle (N12, N13); protonation of the amino group (N15) occurs last according to the results of calculations (Figure 4).

There are two possible stages of protonation of CP-41 nitrogen atoms for the heterocycle protonation without side substituents (Figure 5). Curiously, both the nitrogen atom N6 of the heterocycle and the carbon atom C_1 with a triple bond added a proton as the calculation also predicts. The difference of the protomer energies is several tenths of kcal/mol in favor of protonation by nitrogen.

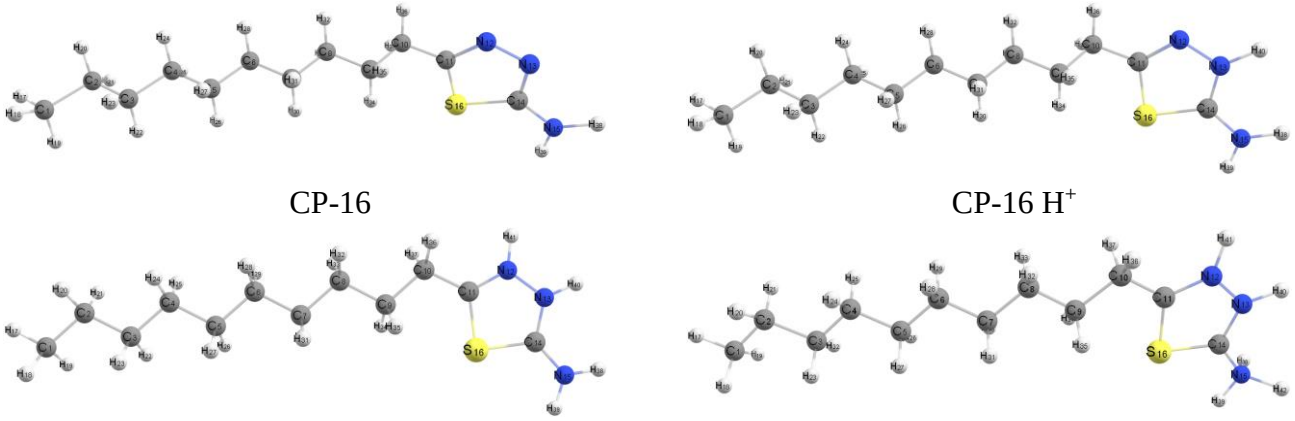

CP-16 CP-16 H^+

CP-16 $2H^+$ CP-16 $3H^+$

Figure 4. Structures optimized at the level of the GFN2-xTB theory [GBSA(H_2O)]: the geometry of a neutral CP-16 molecule and its protonated forms.

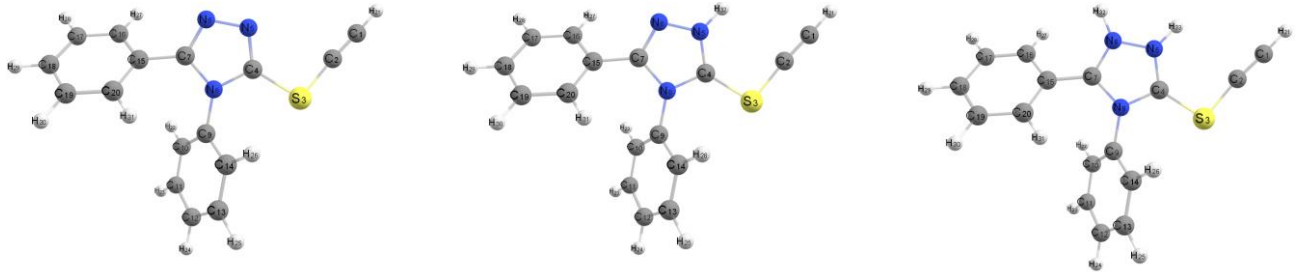

CP-41 CP-41 H^+ CP-41 $2H^+$

Figure 5. Structures optimized at the level of the GFN2-xTB theory [GBSA(H_2O)]: the geometry of a neutral CP-41 molecule and its protonated forms.

There is a possibility of protonation of two nitrogen atoms of the thiadiazole fragment (N13, N14) of CP-44 and an unsubstituted nitrogen atom of the dihydropyrazole fragment (N4). The calculation shows that the N13 atom is protonated first, then N4, and N14 is the last (Figure 6).

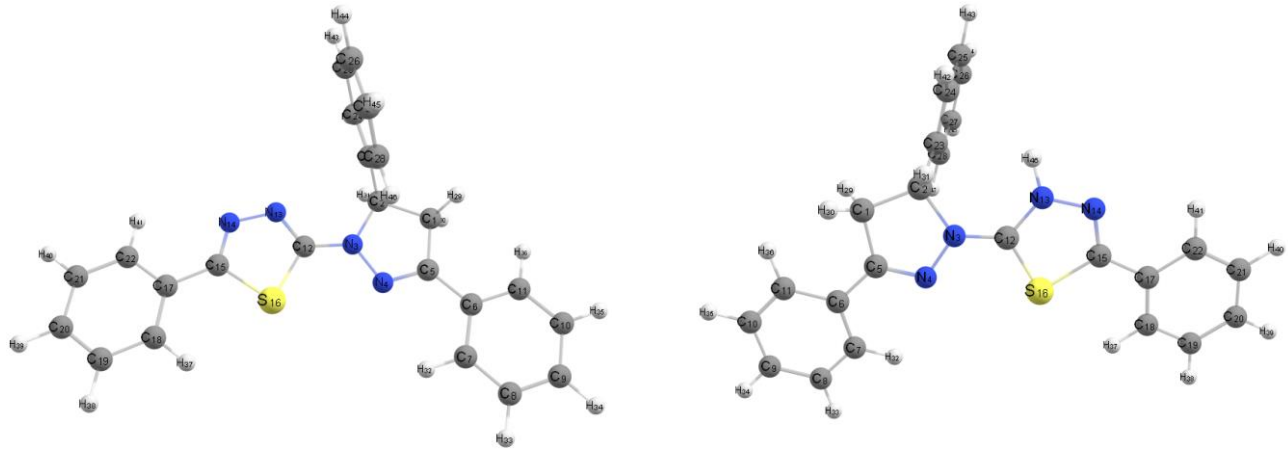

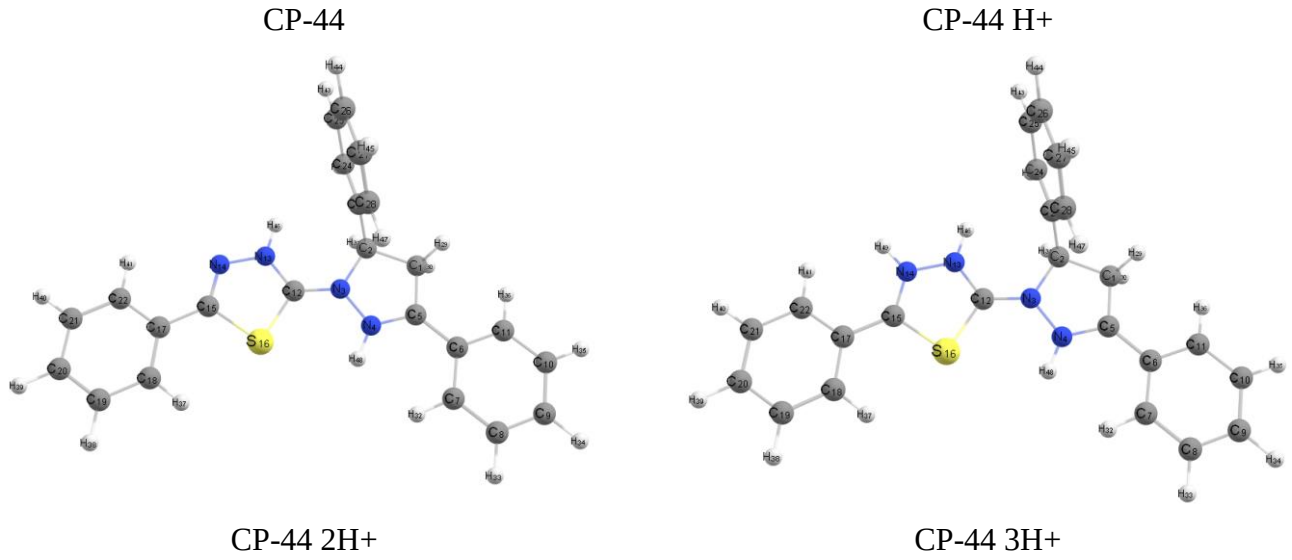

Figure 6. Structures optimized at the level of the GFN2-xTB theory [GBSA(H_2O)]: the geometry of a neutral CP-4 molecule and its protonated forms.

The results of weight loss experiments with the compounds studied in 5 M HCl solution are presented in Table 2.

Table 2. Results of weight loss experiments on mild steel in 5 M hydrochloric acid solution with the inhibitors studied.

Code	C_{inh}, mg/L	K, g/m^2·h	Π, mm/year	Z_{wl}, %	γ
–	–	15.89±0.79	17.62±0.88	–	–
CP-16	50	1.42±0.07	1.57±0.08	91.1±4.6	11.2±0.6
	100	1.07±0.04	1.18±0.05	93.3±3.7	14.9±0.6
	200	1.04±0.04	1.16±0.05	93.4±3.2	15.2±0.5
CP-41	50	3.37±0.13	3.74±0.15	78.8±3.2	4.7±0.2
	100	1.46±0.07	1.62±0.08	90.8±4.5	10.9±0.5
	200	1.41±0.06	1.56±0.07	91.1±3.6	11.3±0.5
CP-44	50	0.57±0.03	0.63±0.03	96.4±4.8	28.0±1.4
	100	0.40±0.01	0.63±0.02	97.5±2.9	39.3±1.2
	200	0.37±0.02	0.63±0.03	97.6±4.9	42.5±2.1

As one can see from Table 2, the protective properties of CP-16 and CP-44 inhibitors practically do not change in the selected range of concentrations. Hence, it can be concluded that the maximum adsorption is established already at 50 mg/L concentration of the inhibitors. However, the inhibition efficiency of CP-41 increases by 10% with an increase in concentration from 50 mg/L to 100 mg/L, then it practically does not change. This

tendency shows that the maximum degree of surface coverage of steel with CP-41 molecules is achieved at a higher solution concentration. CP-44 has the highest inhibitory effect in a 5 M solution of hydrochloric acid (~97% at concentrations >50 mg/L). CP-41 has the smallest protective properties among the compounds studied: the degree of protection varies in the range of 80–90% over the concentration range.

When comparing the results of weight loss measurements and quantum chemical calculations, it can be assumed that the shift of the maximum inhibition efficiency towards lower concentrations is consistent with the different number of heteroatoms in the molecules: CP-16 and CP-44 – three nitrogen atoms, CP-41 – two nitrogen atoms. Similarly, the relatively low protective effect of CP-41 can be interpreted by two competitive equilibrium forms with a proton on N6 or C_1. Thus, each of the forms makes a different contribution to the protective effect. Moreover, the form with protonated nitrogen has a greater protective effect, followed by the form with protonated carbon.

Optical images of a C1018 steel sample are shown in Figure 7.

a

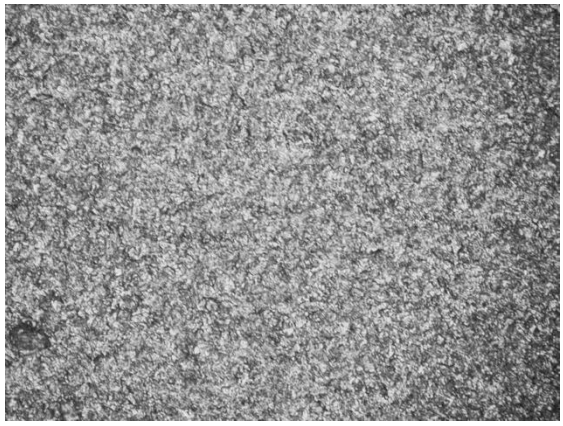

b

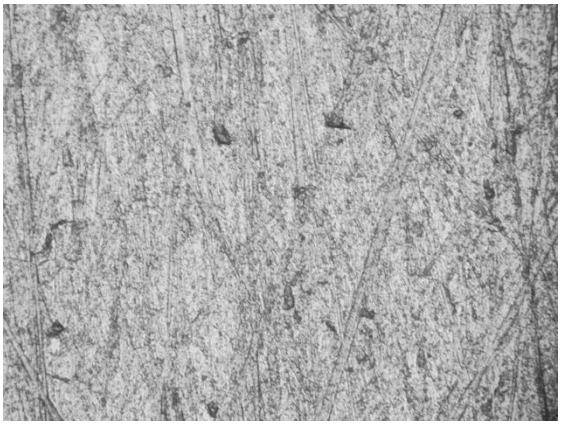

c

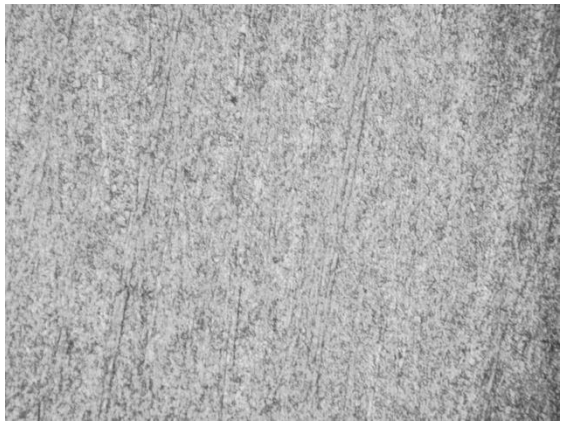

d

e

Figure 7. Optical images of C1018 steel: polished carbon steel (*a*), carbon steel immersed in 5 M HCl (*b*), carbon steel immersed in 5 M HCl with 100 mg/L CP-16 (*c*), CP-41 (*d*), CP-44 (*e*).

The surface of the C-steel shows significant etching after exposing the samples for 24 hours in a 5 M solution of hydrochloric acid. The steel surface remains smoother without pronounced corrosion damage when CP-44 is added to the corrosive environment. CP-16 and CP-41 in the solution significantly reduce surface etching.

Figure 8 shows the polarization curves of a C 1018-electrode in a solution of 5 M HCl without and with addition of 100 mg/L of the potential inhibitors studied.

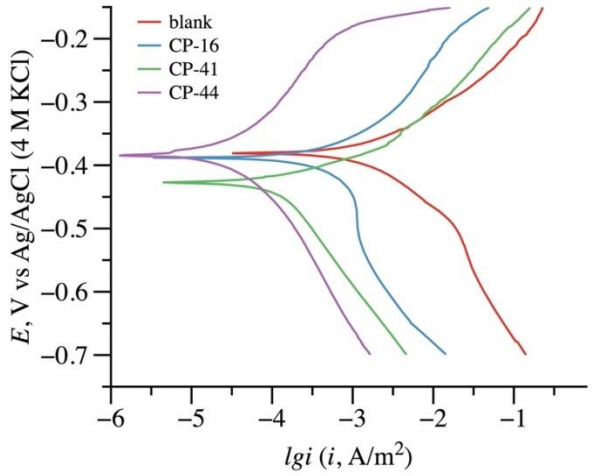

Figure 8. Polarization curves of C1018 steel in 5 M HCl containing of 100 mg/L of the inhibitors at 293 K.

The studied compounds have different effects on the cathodic and anodic partial electrochemical processes [20, 21]. In the case of CP-41, only the cathodic process is inhibited, and in the case of CP-44 and CP-16, both electrochemical processes are inhibited. CP-44 equally affects both processes, but for CP-16, the cathodic process makes a greater

contribution to the protective effect. The corrosion potential of C1018 steel in 5 M HCl solution with CP-16 and CP-44 inhibitors is practically not shifted compared to the non-inhibited solution, while in the case of CP-41, the potential is shifted to the cathodic region.

Based on the polarization measurements obtained, various electrochemical parameters, such as corrosion potential (E_{corr}), corrosion current density (i_{corr}), the coefficients of the Tafel equation, and the inhibition efficiency were calculated and listed in Table 3.

Table 3. Corrosion-electrochemical characteristics of C1018 in hydrochloric acid solutions of various concentrations with addition of 100 mg/L of the inhibitors at different temperatures.

Code	*T*, K	b_a, mV	b_c, mV	$i_{corr}\cdot10^5$, A/cm^2	$-E_{corr}$, V	Z_{el}, %
–	293	39.5±2.0	50.5±2.5	58.44±1.75	0.380±0.019	–
	303	41.8±1.9	63.9±2.6	75.63±1.51	0.372±0.017	–
	313	30.0±1.5	51.9±2.4	116.28±3.37	0.371±0.018	–
	333	27.2±1.4	17.2±0.9	186.14±7.45	0.386±0.021	–
	353	27.5±1.4	28.8±1.7	1165.90±23.32	0.389±0.021	–
CP-16	293	35.5±1.8	54.5±2.5	10.40±0.52	0.386±0.020	82.2±4.1
	303	33.5±1.7	52.1±2.4	14.60±0.73	0.386±0.021	80.7±3.9
	313	24.7±1.4	37.9±1.9	19.70±0.99	0.384±0.019	83.1±4.2
	333	33.2±1.7	45.6±2.4	97.80±4.89	0.386±0.020	47.5±2.4
	353	28.5±1.7	31.2±1.8	1004.21±50.21	0.384±0.016	13.8±0.7
CP-41	293	35.8±1.8	63.3±2.7	6.24±0.31	0.434±0.018	89.3±4.5
	303	30.0±1.7	35.0±1.8	6.83±0.36	0.438±0.022	91.0±4.6
	313	18.6±0.9	46.3±2.3	11.21±0.56	0.440±0.022	90.4±4.2
	333	26.5±1.7	40.6±1.9	56.15±2.81	0.453±0.023	69.8±3.5
	353	28.6±1.7	60.5±2.5	599.50±29.98	0.434±0.021	48.6±2.4
CP-44	293	58.1±2.9	59.2±2.9	1.17±0.06	0.381±0.019	98.0±4.9
	303	55.2±2.4	79.7±3.3	3.13±0.16	0.382±0.019	95.9±4.8
	313	55.8±2.3	68.2±2.9	8.91±0.45	0.381±0.020	92.3±4.6
	333	29.1±1.4	32.0±1.4	14.17±0.71	0.354±0.018	92.4±4.5
	353	32.8±1.7	20.3±1.0	106.18±5.31	0.382±0.017	90.9±4.2

For comparison, the corrosion rate increases with an increase in temperature and only CP-44 retains a high protective effect throughout the temperature range (293–353 K). The degree of protection decreases slightly at 313 K, then practically does not change (Table 3).

In the case of CP-16 and CP-41 inhibitors, the protective properties are reduced by 20–30% when the temperature changes from 313 to 333 K.

Apparently, a physical adsorption process takes place between the inhibitor molecules and the steel surface since the degree of protection is not preserved [22]. From Table 3, the E_a values increase in the presence of nitrogen-containing heterocycles compared to the pure acid solution. Therefore, the adsorption process occurs due to weak Van der Waals interactions at the inhibitor-steel solution interface [23].

Additionally, the protective effect of CP-44 decreases by less than 10% with an increase in temperature, while that of CP-16 and CP-41, by 30–70%. This can be attributed to the fact that in the CP-44 molecule there are significantly more conjugated electron clouds that are responsible for the number of adsorption bonds between the inhibitor and the steel surface.

Table 4. The activation energy of the corrosion process without and in the presence of 100 mg/L inhibitors.

Code	*E*, kJ/mol
–	40.5±2.0
CP-16	45.6±2.1
CP-41	66.3±2.9
CP-44	59.5±1.6

The impedance spectra of C1018 steel in HCl solutions at the corrosion potential E_{corr} are a combination of semicircles of one capacitive arc in the high frequency region and an additional capacitive arc in solutions of CP-16 and CP-44 or an inductive arc in solutions of CP-41 in the low frequency region. In Figures 9–11, *ReZ* is the real component of the impedance and –*ImZ* is the imaginary component of the impedance.

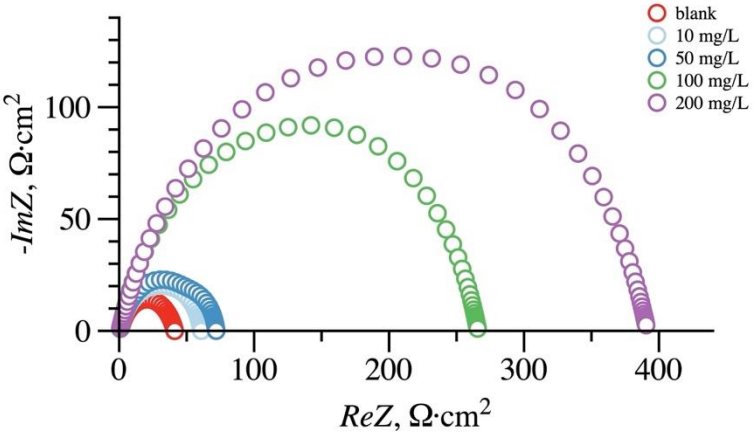

Figure 9. Impedance spectra of C1018 steel in a solution of 5 M HCl at E_{corr} with addition of various concentrations of CP-16.

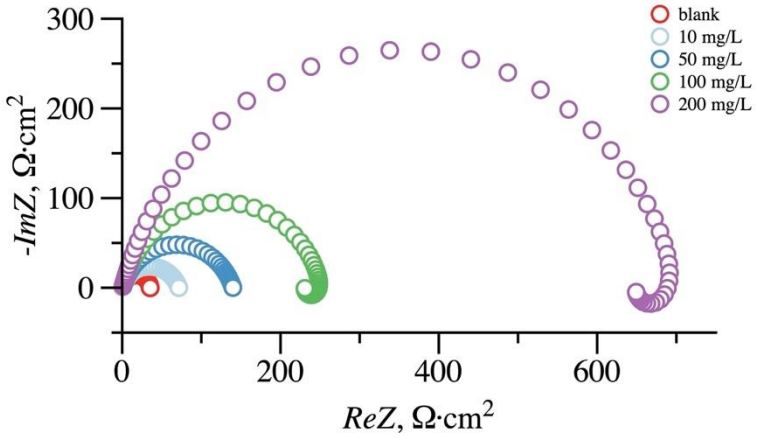

Figure 10. Impedance spectra of C1018 steel in a solution of 5 M HCl at E_{corr} with addition of various concentrations of CP-41.

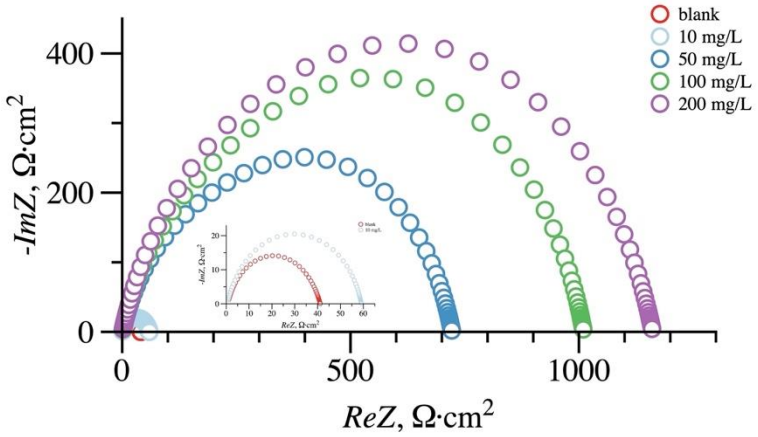

Figure 11. Impedance spectra of C1018 steel in a solution of 5 M HCl at E_{corr} with addition of various concentrations of CP-44.

Addition of the inhibitors to the system causes an increase in the diameter of the capacitive semicircle in the high frequency region, the greater the higher the inhibitor concentration, which is probably due to the hindrance of the electrode reactions.

The equivalent electrical circuit shown in Figure 12 was used to simulate the corrosion-electrochemical behavior of C1018 steel in a solution of 5 M HCl in the presence of CP-16 and CP-44 inhibitors. In this circuit, R_s is the solution resistance; R_1 is the resistance equal to $(R_a \cdot R_c)/ (R_a+R_c)$, where R_a is the resistance of the anodic process (metal dissolution) and R_c is the resistance of the cathodic process (evolution of hydrogen); the resistance R_2 and the capacitance C_1 reflect the adsorption of an intermediate of the anodic process; CPE_1 is a constant phase element describing the capacitance of a double electric layer on an inhomogeneous surface of a solid electrode.

The behavior of the CP-41 inhibitor in 5 M HCl solution is satisfactorily described by the equivalent circuit in Figure 13. In this circuit: R_s, R_1 and CPE_1 have the same physical

meaning as in the circuit in Figure 12; the resistance R_2 and inductance L_1 describe the adsorption of an intermediate of the anodic process.

The values of the χ^2 parameter calculated in ZView2 for the circuits are in the range of $(2–6)\cdot10^{-4}$, which indicates a good correlation with the experimental data.

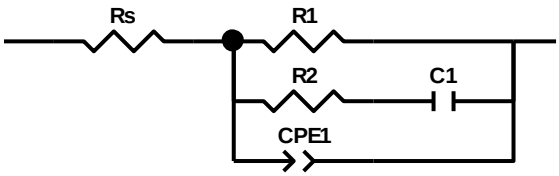

Figure 12. Equivalent electrical circuit for steel C1018 in 1 M HCl solution at E_{cor}.

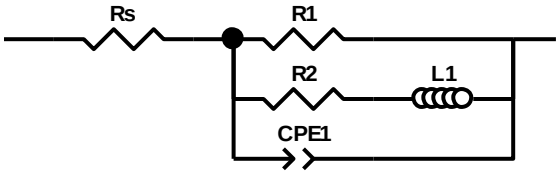

Figure 13. Equivalent electrical circuit for steel C1018 in 5 M HCl solution at E_{cor}.

The parameters of equivalent circuits (Figures 12, 13) for C1018 steel in HCl solutions in the presence of inhibitors are given in Tables 5 and 6.

Table 5. Parameters of equivalent circuits for C1018 steel in 1 M HCl solution without and in the presence of inhibitors.

C_{inh}, mg/L	R_1, Ω·cm²	R_2, Ω·cm²	CPE_1, μF·cm^{-2}·s$^{(p-1)}$		C, μF/cm² / L, H·cm²	θ
			Q	p		
–	40.62±2.03	11.92±0.60	89.88±4.49	0.76±0.01	1.13±0.06	–
			CP-16			
10	60.40±3.02	328.70±16.44	82.36±4.23	0.80±0.01	5.66±0.28	0.75±0.01
50	71.41±3.57	378.60±18.93	77.28±3.98	0.81±0.01	17.51±0.88	0.91±0.01
100	265.50±13.28	1634.21±81.71	68.51±3.43	0.82±0.01	5.14±0.26	0.92±0.01
200	390.93±19.55	2289.43±114.47	52.99±2.65	0.82±0.01	9.50±0.48	0.99±0.01
			CP-41			
10	141.24±7.01	150.43±7.14	80.99±4.37	0.79±0.01	0.05±0.00	0.27±0.01
50	212.95±10.65	404.21±22.17	53.17±2.54	0.77±0.01	0.12±0.00	0.60±0.01
100	252.82±14.32	2591.54±12.96	22.96±0.11	0.77±0.01	815.45±4.08	0.98±0.01
200	706.44±3.53	7913.33±395.67	20.49±0.08	0.79±0.01	8303.12±378.65	0.99±0.01

			CP-44			
10	58.65±2.89	960.21±48.01	65.09±3.25	0.79±0.01	2.03±0.10	0.61±0.01
50	721.70±36.09	2156.97±107.85	20.66±1.03	0.78±0.01	2.01±0.09	0.88±0.01
100	1010.31±50.52	2388.26±119.41	18.70±0.94	0.80±0.01	1.88±0.09	0.97±0.01
200	1205.65±60.28	7687.28±384.36	17.64±0.88	0.81±0.01	0.76±0.04	0.99±0.01

It follows from Table 5 that there is a regular increase in the R_1 and R_2 resistances and a decrease in the Q parameter of the constant phase element CPE_1 (at comparable p values) with an increase in the concentration of the compounds studied. These correlations indicate the inhibition of the electrode processes (mainly the cathodic process) in the presence of the triazoles and their adsorption on the electrode surface. The R_2 and C_1 parameters, along with the interpretation of the adsorption of the intermediate of the cathodic process, can also be associated with the kinetics of the adsorption of compounds on the electrode surface (the Frumkin-Melik-Gaikazyan impedance without a diffusion impedance).

The degrees of surface coverage of the electrode with the inhibitor molecules are approximated in the coordinates of the Langmuir and Freundlich equations [23, 25] (Figure 14, Table 7).

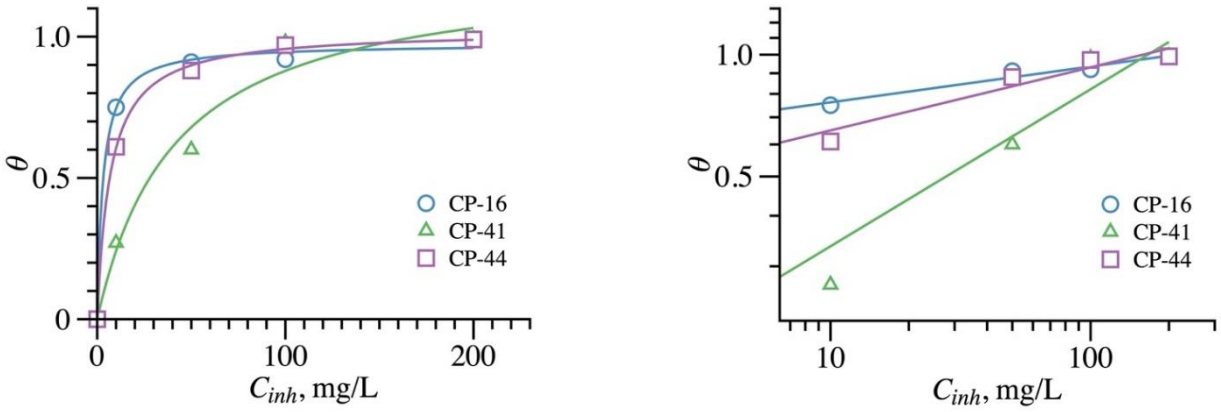

Figure 14. Langmuir (*a*) and Freundlich (*b*) isotherms of adsorption of inhibitors in 5 M HCl solution.

Table 7. Parameters of Langmuir and Freundlich isotherms for the adsorption of CP-20 and CP-38 on the surface of C1018 in HCl solutions.

Code	Langmuir			Freundlich		
	***K*, dm³/g**	***Q*, μmol/m²**	R_2	***K***	***n***	R_2
CP-16	0.3259	0.9747	0.9975	0.6216	0.0886	0.9980
CP-41	0.0240	1.2451	0.9751	0.1375	0.3881	0.9507
CP-44	0.1449	1.0228	0.9992	0.4538	0.1559	0.9893

The values of the correlation coefficients (Table 7) indicate that the adsorption process of the inhibitor obeys the Langmuir isotherm. The adsorption constant of the CP-16 has a high value, indicating greater adsorption of molecules on the surface of C1018, and therefore a better inhibitive ability. However, CP-44 has the best inhibitory effect observed experimentally (Tables 2, 3). Probably, this contradiction can be associated with a steric factor (a large radius of CP-44 molecules), which hinders the sorption of molecules on the metal surface but beneficially affects the protective properties of a potential inhibitor.

Conclusions

- The triazole and thiadiazole derivatives are effective inhibitors of acid corrosion of C1018 steel in 5 M HCl solution.
- According to the results of quantum chemical calculations, the protonation of 1,3,4-thiadiazole containing a tall oil fragment and 2-(3,5-diphenyl-4,5-dihydro-1*H*-pyrazole-1-yl)-5-phenyl-1,3,4-thiadiazole occurs only on nitrogen atoms. Two diprotonated forms are equally possible for 3,4-diphenyl-5-(prop-2-yn-1-ylthio)-4*H*-1,2,4-triazole.
- Nitrogen-containing heterocycles increase the value of the activation energy in 5 M HCl solution; it indicates physical adsorption of the inhibitor molecules.
- According to the polarization results, 1,3,4-thiadiazole containing a tall oil fragment and 2-(3,5-diphenyl-4,5-dihydro-1*H*-pyrazole-1-yl)-5-phenyl-1,3,4-thiadiazole inhibitors are of mixed type, whereas 3,4-diphenyl-5-(prop-2-yn-1-ylthio)-4*H*-1,2,4-triazole is of cathodic type.
- The protective properties 2-(3,5-diphenyl-4,5-dihydro-1*H*-pyrazole-1-yl)-5-phenyl-1,3,4-thiadiazole decreases by less than 10%, but those of 1,3,4-thiadiazole containing a tall oil fragment and 3,4-diphenyl-5-(prop-2-yn-1-ylthio)-4*H*-1,2,4-triazole decrease by 30–70% with an increase in temperature.
- Electrochemical measurements show that the degrees of surface coverage increase with an increase in the inhibitor concentration, causing an increase in the protective effect.
- The Langmuir isotherm model is suitable for describing the adsorption of the inhibitors on the surface of C1018 steel.

Conflict of Interests

The authors declare there is no conflict of interests.

Acknowledgments

Funding: The research was supported by the Perm Research and Education Centre for Rational Use of Subsoil, 2021.

References

1. S.E. Roghayeh, A. Mehdi, M. Soraia, T. Milad, F. Hossein and R. Keyvan, Carboxamide derivatives as new corrosion inhibitors for mild steel protection in hydrochloric acid solution, *Corros. Sci.*, 2019, **151**, 190–197. doi: 10.1016/j.corsci.2019.02.019
2. Yu.I. Kuznetsov, New possibilities of metal corrosion inhibition by organic heterocyclic compounds, *Int. J. Corros. Scale Inhib.*, 2012, **1**, no. 1, 3–15. doi: 10.17675/2305-6894-2012-1-1-003-015
3. M.A. Deyab and Q. Mohsen, Inhibitory influence of cationic Gemini surfactant on the dissolution rate of N80 carbon steel in 15% HCl solution, *Sci. Rep.*, 2021, **11**, 10521. doi: 10.1038/s41598-021-90031-x
4. T. Laabaissi, M. Rbaa, F. Benhiba, Z. Rouifi, U. Pramod Kumar, F. Bentiss, H. Oudda, B. Lakhrissi, I. Warad and A. Zarrouk, Insight into the corrosion inhibition of new benzodiazepine derivatives as highly efficient inhibitors for mild steel in 1 M HCl: Experimental and theoretical study, *Colloids Surf., A*, 2021, **629**, 127428. doi: 10.1016/j.colsurfa.2021.127428
5. A. Zarrouk, B. Hammouti, A. Dafali and F. Bentiss, Inhibitive properties and adsorption of purpald as a corrosion inhibitor for copper in nitric acid medium, *Ind. Eng. Chem. Res.*, 2013, **52**, 2560–2568. doi: 10.1021/ie301465k
6. Y. Qiang, S. Zhang and L. Wang, Understanding the adsorption and anticorrosive mechanism of DNA inhibitor for copper in sulfuric acid, *Appl. Surf. Sci.*, 2019, **492**, 228–238. doi: 10.1016/j.apsusc.2019.06.190
7. X. Li, S. Deng, H. Fu and T. Li, Adsorption and inhibition effect of 6-benzylaminopurine on cold rolled steel in 1.0 M HCl, *Electrochim. Acta*, 2009, **54**, 4089–4098. doi: 10.1016/j.electacta.2009.02.084
8. Yu.I. Kuznetsov and L.P. Kazansky, Physicochemical aspects of metal protection by azoles as corrosion inhibitors, *Russ. Chem. Rev.*, 2008, **77**, no. 3, 219–232. doi: 10.1070/RC2008v077n03ABEH003753
9. Y. Boughoues, M. Benamira, L. Messaadia and N. Ribouh, Adsorption and corrosion inhibition performance of some environmental friendly organic inhibitors for mild steel in HCl solution via experimental and theoretical study, *Colloids Surf., A*, 2020, **593**, 124610. doi: 10.1016/j.colsurfa.2020.124610
10. M.H.O. Ahmed, A.A. Al-Amiery, Y.K. Al-Majedy, A.A.H. Kadhum, A.B. Mohamad and T.S. Gaaz, Synthesis and characterization of a novel organic corrosion inhibitor for mild steel in 1 M hydrochloric acid, *Results Phys.*, 2018, **8**, 728–733. doi: 10.1016/j.rinp.2017.12.039
11. K.F. Khaled, Experimental and molecular dynamics study on the inhibition performance of some nitrogen containing compounds for iron corrosion, *Mater. Chem. Phys.*, 2010, **124**, 760–767. doi: 10.1016/j.matchemphys.2010.07.055

12. K.F. Khaled, Molecular simulation, quantum chemical calculations and electrochemical studies for inhibition of mild steel by triazoles, *Electrochim. Acta,* 2008, **53**, 3484–3492. doi: 10.1016/j.electacta.2007.12.030
13. G. Lei, O. Ime Bassey, Z. Xingwen, S. Xun, Oia. Yujie, K. Savas and K. Cemal, Theoretical insight into an empirical rule about organic corrosion inhibitors containing nitrogen, oxygen, and sulfur atoms, *Appl. Surf. Sci.*, 2017, **406**, 301–306. doi: 10.1016/j.apsusc.2017.02.134
14. M.D. Plotnikova, A.D. Solovyev, A.B. Shein, A.N. Bakiev and A.S. Sofronov, New inhibitors based on substituted 1,2,4-triazoles for mild steel in hydrochloric acid solutions, *Int. J. Corros. Scale Inhib.*, 2021, **10**, no. 3, 1230–1244. doi: 10.17675/2305-6894-2021-10-3-23
15. C. Bannwarth, E. Caldeweyher, S. Ehlert, A. Hansen, P. Pracht, J. Seibert, S. Spicher and S. Grimme, Extended tight-binding quantum chemistry methods, *WIREs Computational Molecular Science*, 2021, **11**, e1493. doi: 10.1002/wcms.1493
16. C. Bannwarth, S. Ehlert and S. Grimme, GFN2-xTB – An Accurate and Broadly Parametrized Self-Consistent Tight-Binding Quantum Chemical Method with Multipole Electrostatics and Density-Dependent Dispersion Contributions, *J. Chem. Theory Comput.*, 2019, **15**, 1652–1671. doi: 10.1021/acs.jctc.8b01176
17. L. Liang, C. Ting-Ting, Z. Qi-Wei and C. Chong-Wei, Organic Phosphorus Compounds as Inhibitors of Corrosion of Carbon Steel in Circulating Cooling Water: Weight Loss Method and Thermodynamic and Quantum Chemical Studies, *Adv. Mater. Sci. Eng.*, 2018. doi: 10.1155/2018/1653484
18. F. Mansfeld, Tafel slopes and corrosion rates obtained in the pre-Tafel region of polarisation curves, *Corros. Sci.*, 2005, **47**, no. 12, 3178–3186. doi: 10.1016/j.corsci.2005.04.012
19. P. Dohare, K. Ansari, M. Quraishi and I. Obot, Pyranpyrazole derivatives as novel corrosion inhibitors for mild steel useful for industrial pickling process: experimental and quantum chemical study, *J. Ind. Eng. Chem.*, 2017, **52**, 197e210. doi: 10.1021/ie300977d
20. O. Devos, C. Gabrielli and B. Tribollet, Simultaneous EIS and in situ microscope observation on a partially blocked electrode application to scale electrodeposition, *Electrochim. Acta*, 2006, **51**, 1413–1422, doi: 10.1016/j.electacta.2005.02.117
21. T. Bochuan, Z. Shengtao, Q. Yujie, G. Lei, F. Li, L. Chaohui, X. Yue and C. Shijin, A combined experimental and theoretical study of the inhibition effect of three disulfide-based flavouring agents for copper corrosion in 0.5 M sulfuric acid, *J. Colloid Interface Sci.*, 2018, **526**, 268–280. doi: 10.1016/j.jcis.2018.04.092
22. R. Solmaz, Investigation of adsorption and corrosion inhibition of mild steel in hydrochloric acid solution by 5-(4-Dimethylaminobenzylidene)rhodanine, *Corros. Sci.*, 2014, **79**, 169–176. doi: 10.1016/j.corsci.2013.11.001

23. K.R. Ansari, M.A. Quraishi and A. Singh, Schiff's base of pyridyl substituted triazoles as new and effective corrosion inhibitors for mild steel in hydrochloric acid solution, *Corros. Sci.*, 2014, **79**, 5–15. doi: 10.1016/j.corsci.2013.10.009
24. T.D. Batueva, M.G. Shcherban' and N.B. Kondrashova, Mesoporous silica materials and their sorption capacity for tungsten (VI) and molybdenum (VI) ions, *Inorg. Mater.*, 2019, **55**, 1146–1150. doi: 10.1134/S0020168519110013
25. S.A. Umoren, I.B. Obot, A.U. Israel, P.O. Asuquo, M.M. Solomon, U.M. Eduok and A.P. Udoh, Inhibition of mild steel corrosion in acidic medium using coconut coir dust extracted from water and methanol as solvents, *J. Ind. Eng. Chem. (Washington, D. C.)*, 2014, **20**, 3612–3622. doi: 10.1016/j.jiec.2013.12.056

♦ ♦ ♦